

See discussions, stats, and author profiles for this publication at: <https://www.researchgate.net/publication/236132555>

Molecular Insight into the Adsorption and Diffusion of Water in the Versatile Hydrophilic/Hydrophobic Flexible MIL-53(Cr) MOF

ARTICLE *in* THE JOURNAL OF PHYSICAL CHEMISTRY C · JUNE 2011

Impact Factor: 4.77 · DOI: 10.1021/jp202147m

CITATIONS

40

READS

132

9 AUTHORS, INCLUDING:



Fabrice Salles

Université de Montpellier

43 PUBLICATIONS 1,212 CITATIONS

[SEE PROFILE](#)



Sandrine Bourrelly

Aix-Marseille Université

48 PUBLICATIONS 3,368 CITATIONS

[SEE PROFILE](#)



Philip L Llewellyn

Aix-Marseille Université

240 PUBLICATIONS 8,184 CITATIONS

[SEE PROFILE](#)



Gérard Férey

Université de Versailles Saint-Quentin

705 PUBLICATIONS 36,726 CITATIONS

[SEE PROFILE](#)

Molecular Insight into the Adsorption and Diffusion of Water in the Versatile Hydrophilic/Hydrophobic Flexible MIL-53(Cr) MOF

Fabrice Salles,[†] Sandrine Bourrelly,[‡] Hervé Jobic,[§] Thomas Devic,^{||} Vincent Guillerm,^{||} Philip Llewellyn,[‡] Christian Serre,^{||} Gérard Ferey,^{||} and Guillaume Maurin^{*†}

[†]Institut Charles Gerhardt Montpellier – UMR CNRS 5253, UM2, ENSCM-Université Montpellier 2, Place E. Bataillon, 34095 Montpellier Cedex 05, France

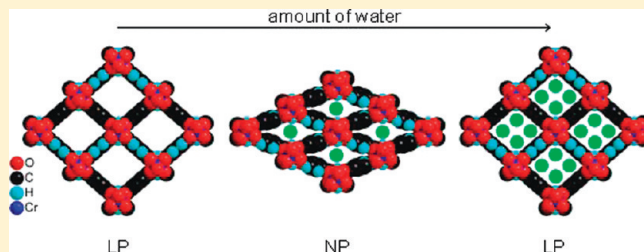
[‡]Laboratoire Chimie Provence, Universités d'Aix-Marseille I, II et III - CNRS, UMR 6264, Centre de Saint Jérôme, 13397 Marseille, France

[§]Institut de Recherches sur la Catalyse et l'Environnement de Lyon, CNRS- Université Lyon 1, UMR 5256, 2 Avenue Albert Einstein, 69626 Villeurbanne Cedex, France

^{||}Institut Lavoisier, UMR CNRS 8180, Université de Versailles Saint-Quentin-en-Yvelines, 45 Avenue des Etats-Unis, 78035 Versailles Cedex, France

 Supporting Information

ABSTRACT: Prior to envisage any implication of metal–organic framework (MOF) materials in industrial applications such as gas storage/separation, it is of primary importance to examine beyond their stability under humidity, the interactions between water and MOF surfaces. Regarding the MOF type MIL-53(Cr), the situation becomes more complex due to the breathing of its structure upon water adsorption that induces a structural transition between a narrow pore (NP) and a large pore (LP) forms. The resulting shrinkage/reopening of the framework leads to crucial modifications of the hydrophobicity/hydrophilicity character of the material. A combination of molecular simulations (Grand Canonical Monte Carlo and molecular dynamics) and experimental techniques (quasi-elastic neutron scattering and gravimetry/volumetry) allows a complete elucidation of the adsorption and diffusion mechanisms in play in this structure. It also provides a microscopic explanation of the hydrophilic and mildly hydrophobic behaviors of the NP and LP forms respectively. The arrangements of water within the two porosities are then discussed and compared to those usually observed for the liquid state. Furthermore, the self-diffusivity for water in these two structural forms significantly differs both in magnitude and mechanism with a normal and single file one-dimensional diffusion mechanisms in the LP and NP forms, respectively. Indeed, this anomalous behavior of the MIL-53(Cr) upon water adsorption implies a strong modification of its hydrophilic/hydrophobic character. This unusual behavior opens a promising direction to improve the selectivity of MOFs in industrial applications such as purification of alcohols without the need for functionalization procedures.



INTRODUCTION

Metal–organic frameworks (MOFs) or porous coordination polymers first appeared at the end of the 1990s.^{1,2} They are a class of hybrid organic–inorganic materials, which are built up from inorganic subunits (transition metals, main group elements, lanthanides, and so forth) and organic moieties (polyphosphonates, polycarboxylates, imidazolates, and so forth). The emergence of novel MOF structures has been almost exponential since the first reporting of MOF-5 by Yaghi et al.^{1,3} Their direct^{4–6} and postsynthetic functionalizations^{3,7–9} have further allowed the preparation of a wide range of hybrid materials, offering a way to both modulate their interactions with different types of guest molecules^{10–15} and to enhance their thermal stability in air^{2,16,17} or water.¹⁸ All these features make them very promising candidates in different areas including gas capture/separation, catalysis and drug encapsulation.^{2,10,11,19–28} However, prior to envisage

any implication of these solids in industrial applications regarding gas adsorption/separation, it is of primary importance to both examine their stability under humidity and to understand the interactions between water and the MOF surface which are known to significantly either alter or improve their adsorption/separation performances with respect to different gases.^{29–33} In that way, the stability of a wide range of MOFs under water atmosphere has already been evaluated.^{18,34} For instance, the Material of the Institut Lavoisier (MIL) series do not show any significant alteration of their porosity upon water adsorption,^{32,33,35} and especially the flexible MIL-53 solid, while some other MOFs including MOF-177, MOF-5, and HKUST-1 are

Received: March 7, 2011

Revised: April 19, 2011

Published: May 06, 2011

unstable.^{36–40} In contrast, only a few experimental adsorption isotherms are available in the literature for such materials^{32,41–44} and the exploration of the interactions between polar molecules, that is, water and alcohols, and the MOF surfaces is scarcely investigated so far.^{31,32,43–45} It has been thus experimentally evidenced that, while most of the investigated MOFs are hydrophilic giving rise to interactions via hydrogen bonds between their pore walls and the polar molecules,^{32–45} some others show a V-type isotherm characteristic of the hydrophobic nature of their surfaces.⁴¹ From a modeling standpoint, most of the studies were concentrated on determining the location of the polar molecules within the porosity of some MOFs using either energy minimization techniques based on classical force fields or quantum calculations.^{32,39,45–47} Exploring the behavior of water confined in nanoporous materials is also of fundamental interest as attested by the large number of studies devoted to this topic since the past few years on different solids including zeolites, mesoporous silicas, activated carbons and more recently on MOFs.^{48–57} In this latter case, Paranthaman et al.⁵⁸ have employed Grand Canonical Monte Carlo simulations to characterize the hydrophobic behavior of the Al(OH)(1,4-naphthalenedicarboxylate) which is a one-dimensional (1D) MOF type material.

Here, one aims at providing molecular insight into the adsorption and diffusion processes of water occurring in the MIL-53(Cr) solid.⁵⁹ This chromium terephthalate (L) formulated Cr(OH)(L) presents a 1D pore system associated with a high structural flexibility either with temperature or pressure^{60–62} or in presence of various guest molecules. This behavior was attributed to a reversible structural switching between a narrow (NP) and a large pore (LP) form, implying variations in cell volume up to 30% in presence of CO₂.^{63–65} This investigation follows a recent study reported by some of us which revealed an anomalous water adsorption behavior of this solid at low pressure that was not fully explained at the microscopic scale.³² A preliminary step consisted of conducting molecular dynamics in the NVT ensemble to validate the force field⁶⁵ selected for representing the MIL-53(Cr)/H₂O interactions, by successfully capturing the two consecutive structural switching upon water adsorption from the LP to the NP forms followed by a reopening of the structure at higher pressure as shown by ex-situ X-ray diffraction (see Figure 1). Grand Canonical Monte Carlo simulations based on this force field were then employed to predict both the absolute adsorption isotherm and enthalpy, which are further compared to gravimetry/microcalorimetry data. The complex shape of the adsorption isotherm at low pressure is then interpreted in light of the structural transitions in play. The resulting modification of the water affinity of the MIL-53(Cr) when one switches from the LP to the NP forms is further discussed by a careful inspection of the microscopic adsorption mechanism for water in the two structures. As far as we know, it is the first time that the hydrophobic/hydrophilic character of a solid can be tuned by a structural transition that leads to the observation of a V-type shape isotherm at low pressure. The so-observed “hydrophobic” character of the LP form is further compared to the water adsorption behavior of its isostructural rigid V(O)(L) or MIL-47(V) counterpart.⁶⁶ In this latter material, the substitution of the μ₂-OH vertices by the μ₂-O groups at the MOF surface is expected to enhance its hydrophobicity. At this point, one emphasizes how the adjustment of the partial charges carried out by the atoms of the hydrophobic MIL-47 framework is a critical step to get a better agreement between experimental and simulated adsorption isotherms. The confinement

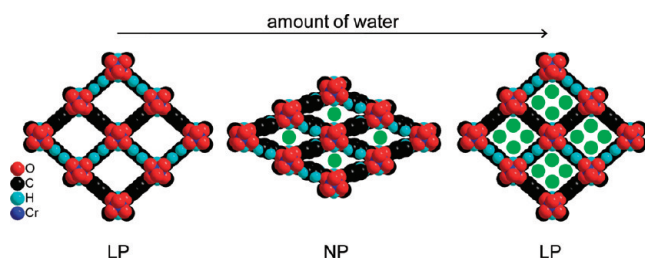


Figure 1. Evolution of the structure of MIL-53(Cr) upon adsorption of water. LP = large pore form, NP = narrow pore form.

effect on the arrangement of the water molecules within the porosity of both MILs is then pointed out by a direct comparison with the microscopic behavior of the same molecule in the liquid state. Finally, molecular dynamics is coupled with quasi-elastic neutron scattering experiments in order to shed some light into the dynamics of water in these hybrid materials, which has not been addressed so far in any MOF type solids.

MATERIALS AND METHODS

Sample Preparation. MIL-53(Cr) and MIL-47(V) were synthesized and activated according to the published procedures.^{59,63,66} Hydrogenated samples were used for the isotherm measurements, whereas deuterated MIL-53(Cr) was selected for the neutrons scattering experiments. This latter was prepared from d4-terephthalic acid (Euristostop, France) and hydrogenated solvent as already reported.⁶⁷

Adsorption Measurements. The adsorption isotherms were obtained by gravimetry measurements. The laboratory-made adsorption apparatus includes a symmetrical balance and allows a continuous introduction of vapor to the sample in a slow enough manner to ensure quasi-equilibrium between the vapor and the solid and a high-resolution isotherm plot.³² For each series of experiments, this quasi-equilibrium condition is verified by stopping the vapor introduction and ensuring that no change in pressure or mass is observed. A typical adsorption–desorption isotherm takes around 10 days. To carefully measure the desorption of the water vapor from the fully hydrated MIL-47(V), a new experimental procedure was used³² in which the porous solid is initially immersed in an excess of liquid and then slowly evacuated under controlled vacuum conditions, usually through a capillary toward vacuum.

Quasi-Elastic Neutron Scattering. The quasi-elastic neutron scattering (QENS) measurements were performed on the time-of-flight spectrometer IN6, at the Institut Laue-Langevin, in Grenoble, France. The incident neutron energy was taken as 3.12 meV, corresponding to a wavelength of 5.1 Å. Once scattered by the sample, the neutrons are analyzed as a function of flight time and angle. Groupings of spectra were made outside the Bragg peaks of MIL-53(Cr), the average wavevector transfer, Q , ranging from 0.27 to 1.6 Å^{−1}. The line shape of the elastic energy resolution could be fitted by a Gaussian function, whose half-width at half-maximum (HWHM) varied from 40 μeV at small Q to 50 μeV at large Q . After measuring the scattering of the empty MIL, different water concentrations were adsorbed in situ at 300 K, starting from the LP form. After the second loading, the transition to the NP form was observed. The water concentrations were determined from a comparison of the equilibrium pressures with an adsorption isotherm. The largest loading

corresponded to 6 H₂O/uc (unit cell), so that the reopening of the structure was not observed.

■ COMPUTATIONAL METHODS

Microscopic Models and Force Fields. The periodic models of the MIL-47(V) and the large pore (LP) form of MIL-53(Cr) were built using the atomic coordinates available in the literature^{59,66} while the partial charges of both MILs were taken from our preliminary density functional theory (DFT) calculations.⁶⁷ The 12-6 Lennard-Jones (LJ) interatomic potential parameters and the intramolecular terms for describing the flexible MIL-53(Cr) come from our previous study which has successfully captured the breathing of this solid in presence of CO₂.⁶⁵ The 12-6 LJ parameters for the MIL-47(V) were also taken from our recent investigation.⁶⁷

The water molecule was treated by the TIP4P-2005 model developed by Abascal and Vega.⁶⁸ Such a four-site model has been successfully used to reproduce the experimental vapor–liquid phase equilibrium data. The corresponding partial charges expressed in electron units are 0.5564, 0, and 1.1128 for the H, O, and M ((placed on the bisector of the HOH angle at 0.1546 Å from the oxygen) sites, respectively. The LJ term is centered only on the oxygen nucleus.

The adsorbate/adsorbent LJ interatomic potential parameters were then calculated using Lorentz–Berthelot mixing rules.

Molecular Dynamics. Molecular dynamics (MD) simulations were performed using the DL_POLY_2.19 program⁶⁹ in the N_oT ensemble, which was able to simulate both the size and shape changes. The Berendsen and Nosé-Hoover thermostats and barostats were considered for the calculations with the same relaxation times as used in our previous simulations.⁶⁵ MD simulations were first conducted at 300 K starting with the empty LP structure of the MIL-53(Cr) loaded by a number of water molecules ranging from 0.5 to 8 per unit cell, in order to follow the evolution of the structural features of this material as a function of the water content. Each MD was run for 2 ns with a time step of 1 fs, using 32 unit cells to get good statistics and the critical size in order to maintain a consistent cutoff distance of 12 Å ($r_c < L/2$, L = the smallest length of box) during the whole MD simulations. The electrostatic interactions were calculated using the Ewald summation.⁷⁰ The SHAKE-RATTLE and the usual Velocity Verlet algorithms were used to constrain rigid bonds and to integrate the equations of motion. The water molecule was maintained as rigid and the QUATERNION algorithm was used to treat the motion of the adsorbate while the framework was considered as flexible, consistent with our previous study.⁶⁵

The diffusion process of water was further explored by means of MD simulations run in the NVT ensemble using the Nosé-Hoover thermostat at 300 K for both rigid LP and NP forms. Different water contents ranging between 0.5 to 4 and 0.5 to 8 H₂O molecules per unit cell in the NP and LP forms respectively are investigated. The structure generated by the MD calculations in the N_oT ensemble for 5 H₂O/uc, was considered as an “average” one that can fairly represent the NP form in the whole range of pressure explored for this structure. The framework atoms of both NP and LP structures were then maintained fixed during the MD simulations. We have previously pointed out that this assumption does not affect the diffusivity of other adsorbate species within the porosity of this structure.^{67,71} For each loading, the initial configurations were generated by preliminary Monte Carlo simulations in the NVT ensemble. MD simulations were

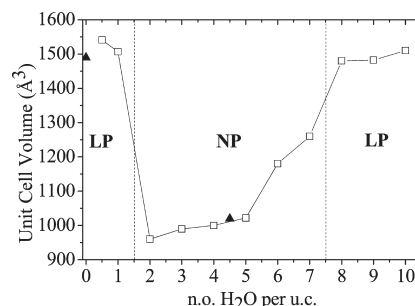


Figure 2. Evolution of the unit cell volume of the MIL-53(Cr) structure as a function of the number of adsorbed water molecules per unit cell, obtained by molecular dynamics simulations (empty squares) at 300 K. For comparison, the experimental values are reported when available (full triangles). The distinction between the LP and NP forms is provided.

then run for 10 ns (i.e., 10×10^6 steps with a time step of 1 fs) after 1 ns of equilibration. The configurations were further stored every 3000 timesteps. The self-diffusivities D_S were then determined for each investigated H₂O concentration (c) using Einstein relations⁷² as reported in eq 1

$$D_S(c) = \lim_{t \rightarrow \infty} \frac{1}{6t} \left\langle \frac{1}{N} \sum_{j=1}^N \| r_j(t) - r_j(0) \|^2 \right\rangle \quad (1)$$

In this equation, $\langle \dots \rangle$ denotes an ensemble average, $r(t)$ are the positions of the tagged guest molecule while N corresponds to the number of H₂O molecules in the simulation volume. Further, in order to improve the statistics of the calculation, multiple time origins, as described elsewhere,⁷² were used while the D_S values were averaged over 5 independent trajectories. Complementary MD simulations were performed at different temperatures in the range [300–500 K] for a loading of 2 H₂O/uc in order to extract the activation energies from the linear least-squares fit to the Arrhenius plots of $\ln(D_S) = f(1000/T)$.

The rotational dynamics for water molecules in the MIL-53(Cr) was further determined from these MD runs by calculating the orientational autocorrelation function $A(t)$ defined by eq 2

$$\langle A(0)A(t) \rangle = \frac{5}{8} \langle (3 \cos^2 \theta(0) - 1)(3 \cos^2 \theta(t) - 1) \rangle \quad (2)$$

where θ is the angle between the molecular end-to-end vector and the MOF coordinate system. Instead of using a fit of the autocorrelation function with three exponential components as proposed by Saengsawang et al.,⁷³ we considered here the time at which the autocorrelation function drops down to 1/e as the characteristic average time for the rotational reorientation of the molecule, following the same approach reported by Wehring et al.⁷⁴

Grand Canonical Monte Carlo Simulations. Grand Canonical Monte Carlo (GCMC) simulations were performed by means of the Complex Adsorption and Diffusion Simulation Suite (CADSS) code⁷⁵ with typically 2.0×10^8 Monte Carlo steps following 1.5×10^7 steps for equilibration. The Ewald summation was also used for calculating the electrostatic interactions while the short-range contributions were computed with a cutoff distance of 12 Å to be consistent with MD calculations. The simulations were conducted at 300 K using both the NP and LP structures as rigid, considering simulation boxes as 32 unit cells that allowed us to evaluate the

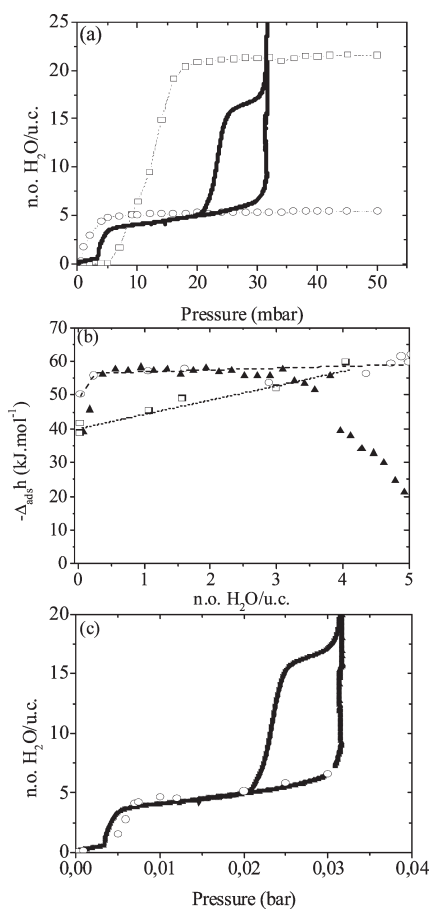


Figure 3. (a) Simulated H₂O absolute adsorption isotherms at 300 K for the LP (open squares) and NP (open circles) compared to the gravimetry data (triangles). (b) Calculated and experimental H₂O adsorption enthalpy following the same labels than in (a). (c) Comparison between the composite adsorption isotherm (open circles), built from the simulated isotherms obtained individually for the LP and NP forms and the (LP, NP) fractions estimated from infrared spectroscopy³² and the experimental gravimetry adsorption isotherm (solid lines).

absolute adsorption isotherms and the adsorption enthalpies. A composite approach that we already successfully employed for other gases^{12,64,71} in this material, was further considered to describe a simulated adsorption isotherm in the whole range of pressure by considering the isotherms calculated in both rigid LP and NP forms and the fractions of the two forms present along the pressure range that were taken from previously reported infrared measurements.^{32,64,65}

RESULTS AND DISCUSSION

The structural evolution of the MIL-53(Cr) solid (see Figure 1) upon water adsorption was first investigated using N_oT MD simulations based on the force field described above. Figure 2 summarizes the simulated unit cell volumes for MIL-53(Cr) as a function of the water loading which varies from 0.5 to 8 H₂O molecules/uc in order to span the whole pressure range of the adsorption isotherm (Figure 3a). For 0.5 and 1 H₂O/uc, the structure remains in its initial LP form with a unit cell volume at 1510 Å³ very close to the one simulated in absence of water (1490 Å³) that further compares very well with the experimental

one (1486 Å³). A drop in the unit cell volume occurs for 1.5 H₂O/uc attaining a value of 950 Å³, consistent with a NP form.⁵⁹ For 5 H₂O/uc corresponding to the adsorbed amount on the first plateau of the experimental adsorption isotherm (Figure 3a), the structure is still in its NP version with a unit cell volume of 1012 Å³, which is in very good agreement with the one previously determined by ex-situ X-ray diffraction for similar loading (1020 Å³). Further, above 5 H₂O/uc, an expansion of the unit cell volume occurs, suggesting a progressive swelling of this form, as emphasized for other guest molecules.^{63,65} This is not experimentally confirmed in this case since the ex-situ X-ray diffraction measurements were not performed continuously in the whole range of pressures investigated by the simulations. The structure then returns to the LP form for 8 H₂O/uc with a simulated volume of 1475 Å³ very close to the initial empty form. Indeed, our simulations predict the predominance of the LP form at very low loading and above 5 H₂O/uc, while the NP version is present in the intermediate range of loading. In addition to the agreement between the simulated unit cell volume and the experimental one available for two loadings, these conclusions are also consistent with the presence of substeps in the isotherms around 1 and 6 H₂O/uc assigned to the two consecutive structural switchings from LP to NP and from NP to LP (see Figure 3a). At higher loadings, the unit cell volumes slightly increase. This result is also consistent with the recent findings reported by Guillou et al.⁷⁶ that determined a unit cell volume of 1550 Å³ for the superhydrated LP structure. This whole set of data allowed us to validate the force field used here to describe the intermolecular water/water and water/MIL framework interactions in complement to the intramolecular interactions within the MIL-53(Cr) framework.

A further step consisted of simulating the adsorption isotherms and enthalpies for the rigid NP and LP forms at 300 K (see Figures 3) using the so-validated force field. Figure 3a reports the two simulated isotherms for pressures varying from 0 to 50 mbar, close to the saturation pressure at 300 K (~37 mbar). One can observe the following two distinct behaviors: while the adsorption isotherm calculated for the NP form presents a rapid increase of the adsorbed amount up to a saturation of 5 H₂O molecules/uc, the adsorption in the LP form starts with a very small uptake at low pressure (5 mbar) leading to the presence of a plateau, followed by a sudden increase up to reach 21 H₂O/uc at 40 mbar. In this latter case, one obtains a type-V isotherm usually observed for systems where the adsorbate/adsorbent interaction is rather weak. Indeed, the interaction between the water molecules and the MIL-53(Cr) framework at low pressure strongly differs in both forms. This different behavior is also confirmed from an energetic point of view. As observed in Figure 3b, the adsorption enthalpies calculated at low coverage significantly deviate with values centered around -50 and -39 kJ·mol⁻¹ for the NP and the LP forms, respectively, that need to be compared to the vaporisation enthalpy for water (~ -44 kJ·mol⁻¹)⁷⁷ at room temperature. Both isotherm and enthalpy profiles simulated for the LP form in the low domain of pressure thus suggest a soft hydrophobic-like behavior of this structure while the water adsorption is favored in the NP version. It results that such a water-assisted structural transition drastically modifies the hydrophobic/hydrophilic character of the MIL-53(Cr) material. The comparison of these simulated data with both experimental adsorption isotherm and enthalpy (Figure 3a,b), recently reported by some of us,³² is then employed to validate such findings. One first observes that the experimental adsorption

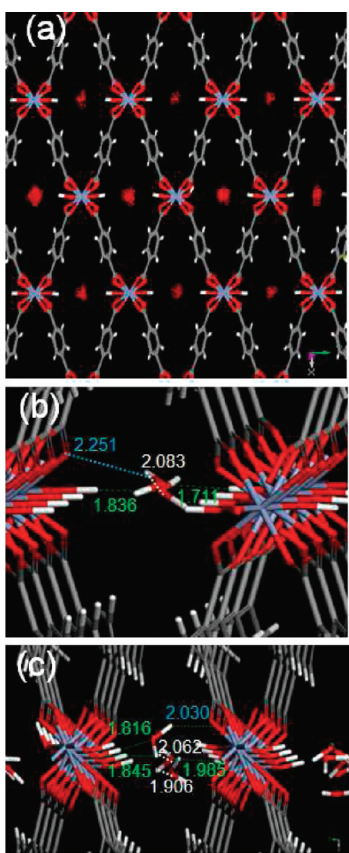


Figure 4. The 2D density plots for water in the NP form of MIL-53(Cr) at 300 K obtained from GCMC simulations through the xy plane for 1 $\text{H}_2\text{O}/\text{uc}$. Red regions correspond to the higher probability of containing H_2O molecules (a). Typical arrangements of the water molecules in the NP form obtained at low (1 mbar) (b) and high loadings (10 mbar) (c). The distances (in Å) reported in green and blue correspond to the interactions between the water molecules and the MOF framework while those in white are between water molecules.

isotherm shows two steps, confirming small uptake at very low pressure with the presence of a plateau that corresponds to the adsorption occurring initially in the LP form. Such “hydrophobic” character of the MIL-53(LP) form is also confirmed by the very low experimental adsorption enthalpy measured at the initial stage of adsorption ($-35 \text{ kJ} \cdot \text{mol}^{-1}$)³² (Figure 3b) in agreement with the simulated value ($-39 \text{ kJ} \cdot \text{mol}^{-1}$), which both remain significantly below the vaporisation enthalpy. For the pressure range comprised between 7 and 30 mbar, the experimental isotherm is well described by the simulated one for the NP structure (Figure 3a), which supports that this form is predominantly present in this range of pressure as claimed above. One notices that the adsorbed amount does not reach a plateau but rather continuously increases, consistent with the predicted progressive swelling of the NP form as reported by Figure 2. Further, the experimental adsorption enthalpy reaches in this range of pressures a plateau around $-58 \text{ kJ} \cdot \text{mol}^{-1}$ which is in agreement with the value calculated for the water adsorption in the NP form ($-55 \text{ kJ} \cdot \text{mol}^{-1}$) (Figure 3b). Above 30 mbar, the isotherm shows a sudden uptake which corresponds to the second structural switching (from the NP to the LP form) as discussed above.

In order to quantitatively analyze the experimental adsorption isotherm and more particularly in the two transition regions where both LP and NP forms can coexist, a “composite” approach is required. It is based on the determination of a global adsorption isotherm from those calculated individually in both rigid NP and LP forms using eq 3

$$N^{\text{sim}}(p) = X_{\text{LP}}^{\text{sim}}(p)N_{\text{LP}}^{\text{sim}}(p) + X_{\text{NP}}^{\text{sim}}(p)N_{\text{NP}}^{\text{sim}}(p) \quad (3)$$

where $X_{\text{LP}}(p)$ and $X_{\text{NP}}(p)$ are the fractions of the LP and NP forms respectively for a given pressure p , that have been previously extracted from infrared measurements,³² $N_{\text{NP}}(p)$ and $N_{\text{LP}}(p)$ are the adsorbed amounts of H_2O simulated in the NP and LP rigid forms respectively and $N(p)$ the total uptake for a given pressure p . The resulting simulated “composite” adsorption isotherm is in good agreement with the experimental one obtained by gravimetry (note that, for the high pressure range, the comparison is made with the experimental desorption branch as seen in Figure 3c). Our simulations predict a pressure for the first structural LP to NP transition slightly shifted compared to the experimental one. This deviation can be explained by the fact that our calculations are based on the NP/LP fractions estimated by infrared spectroscopy whose equilibrium conditions can slightly differ from those considered during the gravimetry measurements.³²

Such behaviors could be rationalized by simply looking at the exposure of the hydrophilic (inorganic part) and hydrophobic (aromatic ring) parts of the framework (see Figure 1). Whereas both parts are accessible toward guests in the LP form, the NP form presents rather segregated hydrophobic and hydrophilic portions, associated with an almost close packing of the phenyl rings which becomes less accessible toward guests. To get some insights into the microscopic adsorption mechanism, the probability density of water in the pore of the NP form was calculated from the analysis of the configurations stored during the GCMC simulations. At low loading, the water molecules are homogeneously distributed within all the pores of the MIL-53(Cr) as shown in Figure 4a. Further, in addition to the hydrogen bonds they establish between each other, the water molecules interact strongly with the two opposite pore walls of the material via hydrogen bonds between (i) their oxygen atoms O_w and the protons of the $\mu_2\text{-OH}$ groups and (ii) their protons H_w and the oxygen atoms of the carboxylate groups as illustrated in Figure 4c. It is clearly stated from the radial distribution functions calculated at low loading for the $\text{O}_w\text{-O}_w$ pair (Figure 5a) that the hydrogen bonds are slightly stronger than in the bulk state with characteristic mean $\text{O}_w\text{-O}_w$ distances of 2.6 and 2.8 Å⁶⁸ respectively. One can further notice from Figure 5b that the average $\text{O}_w\text{-H}(\mu_2\text{-OH})$ distances (1.6 Å) are shorter than the ones between the water molecules ($\text{O}_w\text{-H}_w$ of 1.9 Å). This means that the interactions between the water molecules and the MIL-53(Cr) surface are stronger than those in play between the water molecules themselves, which is in agreement with a higher acidity of the $\mu_2\text{-OH}$ group. Moreover, the water molecules are highly orientated along the direction of the tunnel whatever the loading, as illustrated in Figure 4b,c for different loadings. These resulting geometries are consistent with those previously reported by DFT calculations and ex-situ X-ray diffraction.³²

The situation drastically differs in the case of the LP form of the MIL-53(Cr). One first observes that the water molecules are not homogeneously distributed within all the pores of the material at the low pressure. As a typical illustration, Figure 6a

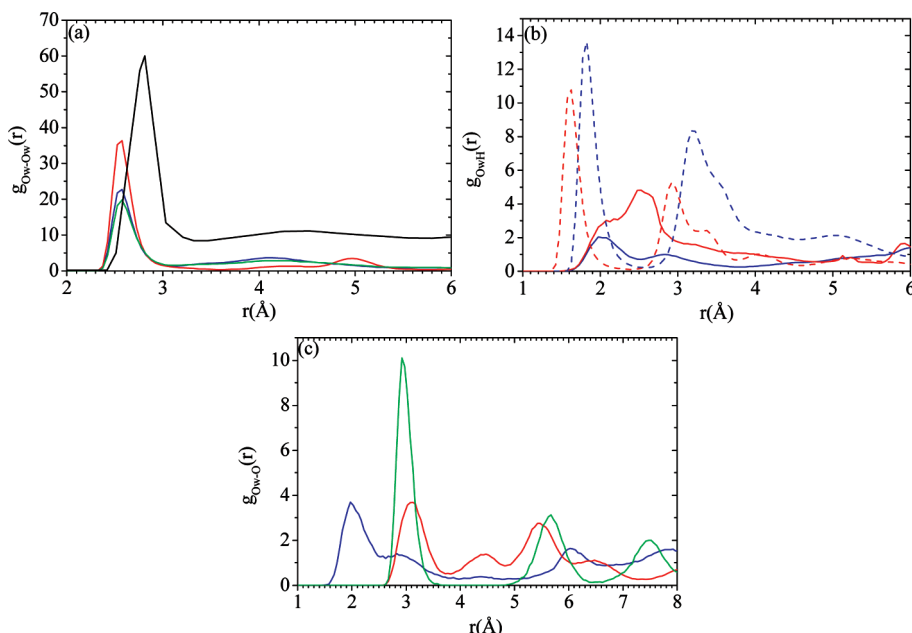


Figure 5. Radial distribution functions for O_w–O_w interactions (O_w for oxygen water) in MIL-53(Cr)-LP and -NP, MIL-47(V) and bulk water (a), O_w–H(μ_2 -OH) (dash lines) and O_w–H_w (straight lines) in MIL-53(Cr) LP and NP (b), and O_w–O(μ_2 -OH or -O) in MIL-53(Cr)-LP and NP and in MIL-47(V) (c) at low loading. The blue, red, and green lines correspond respectively to the MIL-53(Cr)-LP, -NP and MIL-47(V). The bulk water is represented by black lines.

clearly shows that only one pore is partially filled while the others are almost empty that is consistent with a soft hydrophobic character of this structure as mentioned above. When the pressure increases, the filling of the pores occurs in such a way that the water molecules form small clusters instead of interacting each with the pore wall (Figure 6b,c). This is mainly due to stronger water/water interactions compared to the H₂O/MIL surface (see RDFs in Figure 5), as already observed in the case of the adsorption of water and alcohol in silicalite⁷⁸ and in ZIF,⁴⁴ respectively. Indeed, there is only limited intermediate filling state of the channel although one observes some transitional intervals when the pore gets filled (Figure 6a). Such a behavior has already been reported for water in several zeolites^{55,75} and more recently in the MOFs.^{58,79–81} At higher pressure, the hydration mechanism imposes a water cluster-growth adsorption process similarly to the case of silicalite or NaA^{55,82,83} and typically accepted as the water adsorption mechanism in most porous solids.⁸⁴ Typical configurations are provided in Figure 6c at high loadings with the formation of a cluster constituted by 10 H₂O molecules with a cylindrical/spherical shape in a similar way than in the liquid phase where up to 14 water molecules are implicated in the formation of the tetrahedral clusters.⁸⁵ Such an arrangement is in good agreement with those recently elucidated in this material by ex-situ X-ray diffraction experiments.⁷⁶ At the saturation, up to 2.5 hydrogen bonds per water molecules can be formed in this LP form. Although this number is larger than those calculated at the saturation in the NP form (1.8), it remains lower than in the bulk water (3.6 hydrogen bonds).⁸⁶

If one compares now this behavior with those observed in the isostructural MIL-47(V) where the μ_2 -OH sites of the LP form are substituted by the μ_2 -O group with a lower affinity for water, one would expect a more pronounced hydrophobic character of the MIL surface. This behavior is consistent with previous studies in silicalite where the presence of chemical defaults leads to the

change of the affinity of this zeolite from an hydrophobic to a hydrophilic character.⁷⁸ One can thus suspect that the presence of the μ_2 -OH group plays a similar role allowing the water molecules to initiate the formation of clusters and condensate. Such statement would result on a fully hydrophobic character of the MIL-47(V) structure that is confirmed by our simulations (Figure 7). Indeed, the distribution of water molecules is strongly heterogeneous, as shown in Figure 7a, with either completely empty or filled pores, consistent with the behavior previously pointed out in several zeolites including silicalite-1 and DAY qualified as hydrophobic solids.⁸⁷ This trend remains true up to high pressures. As confirmed by the RDF plots in Figure 5c, the interactions between the H₂O molecules and the pore wall of MIL-47(V) is comparable to those observed for the MIL-53-(Cr)-LP. The water molecules are then arranged in a such a way to form clusters within the center of the porosity. They are constituted by up to 12 H₂O at high loading as illustrated in Figure 7c. This situation becomes more similar to the number of water molecules implicated in the clusters (14 for tetrahedral clusters) for the bulk water, while the number of hydrogen bonds between water molecules at saturation (2.9) remains lower than in the bulk phase.

The simulation of the adsorption isotherms in the case of MIL-47(V) imposes to rescale the partial charges. Indeed, as seen in Figure 8a, the comparison between experimental data and simulated results shows a large discrepancy if we consider the previous partial charges validated for CH₄ and CO₂ adsorption and diffusion.^{64,65,67} As suggested previously by other authors,^{57,58,88,89} one way to take into account that the water adsorbed in porous solids is in a less polarizing media than in bulk water consists of adjusting the partial charges of the atoms of the pore wall, which allows one to simulate correctly the condensation of water in hydrophobic solids before the saturation pressure. Here, four different charges distributions were tested: 100 (if we consider

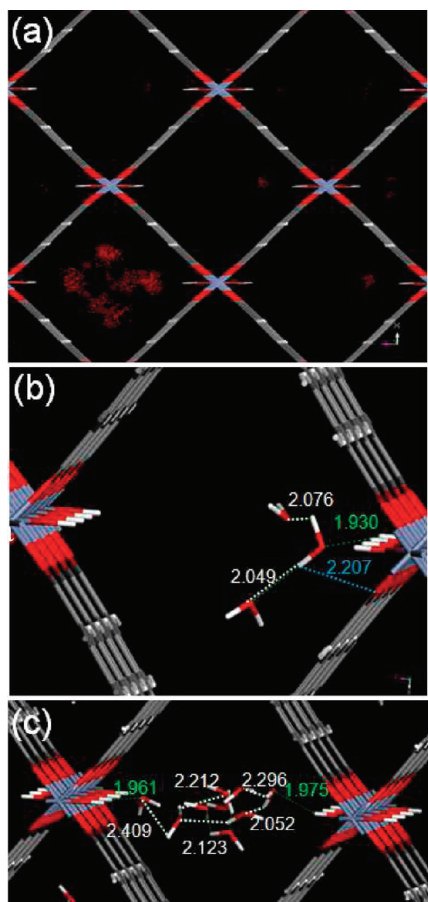


Figure 6. The 2D density plots for water in the LP form of MIL-53(Cr) at 300 K obtained from GCMC simulations through the yz plane for 1 $\text{H}_2\text{O}/\text{uc}$. Red regions correspond to the higher probability of containing H_2O molecules (a). Typical arrangements of the water molecules in the LP form obtained at low (2 mbar) (b) and high loadings (15 mbar) (c). The distances (in \AA) reported in green and white correspond to those separating the water molecules and the framework and between water molecules themselves, respectively. In blue, additional information is reported for distance between the water molecules and the oxygen of the carboxylate groups.

the partial charges calculated by Rosenbach et al.⁶⁷), 70 (if we consider only 70% of all the partial charges from Rosenbach et al.⁶⁷), 50, and 30%. It comes that the calculations performed with 30% of the initial charges reproduce better the experimental condensation zone (15–33 mbar vs \sim 30 mbar) (Figure 8a). An additional charge distribution, already proposed to simulate the adsorption of alkanes in MIL-47(V),⁹⁰ has also been tested but it does not improve the description of the experimental data (see Supporting Information Figure S1), predicting a condensation at higher pressure.

We should note that in the case of the hydrophilic NP form of MIL-53(Cr) material, there is no need to rescale the charges to modulate the water–pore wall interaction as attested by the very good agreement between experimental and simulated low coverage enthalpies. For consistency, the LP form is also simulated using the same partial charges. The comparison of the isotherm obtained for MIL-47(V) and the MIL-53(Cr)-LP is given in the Figure 8b. One clearly shows that the hydrophobic character is less marked in the MIL-53(Cr)-LP form than in MIL-47(V), where the hydration process starts only at

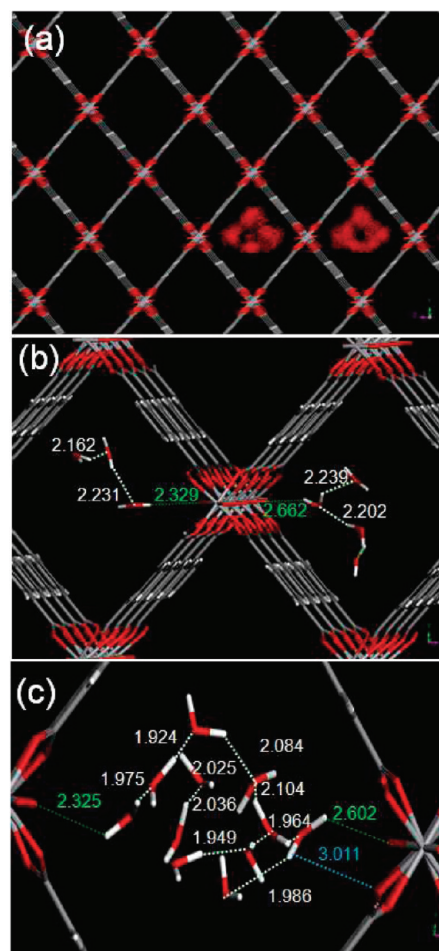


Figure 7. The 2D density plots for water in the MIL-47(V) (a) at 300 K obtained from GCMC simulations through the xy plane obtained for 1 $\text{H}_2\text{O}/\text{uc}$. Red regions correspond to the higher probability of containing H_2O molecules. Typical arrangements of the water molecules in the MIL-47(V) at low loading (10 mbar) (b) and high loading (40 mbar) (c). The distances (in \AA) reported in green and white correspond to distances between water molecules—framework and between water molecules—water molecules, respectively. In blue, additional information is reported for distance between water molecules and carboxylate oxygens.

30 mbar in MIL-47(V) (vs 15 mbar in the LP structure), that is, closer to the saturation pressure of water.

Molecular dynamics simulations were further employed at 300 K to explore the concentration dependence of the self-diffusivity (D_S) for water in the two MIL-53(Cr) forms. The corresponding evolutions of D_S as a function of the loading are provided in Figure 9. Note that the reported D_S correspond to orientationally averaged values, while the MSD plots show that the displacements mainly occur along the direction of the tunnel. One observes that D_S decreases gradually when the loading increases for both forms. Such decreasing D_S profiles are explained by the decrease of the free space available for the diffusion combined to an increase of the water/water interactions when the adsorbate concentration increases. Further, the diffusivity remains faster in the LP form within the whole range of water loading with D_S values ranging from 8×10^{-10} to $1.5 \times 10^{-11} \text{ m}^2 \cdot \text{s}^{-1}$ and from 10^{-9} to $2.5 \times 10^{-11} \text{ m}^2 \cdot \text{s}^{-1}$ in the NP and LP versions, respectively. This result is not surprising as the

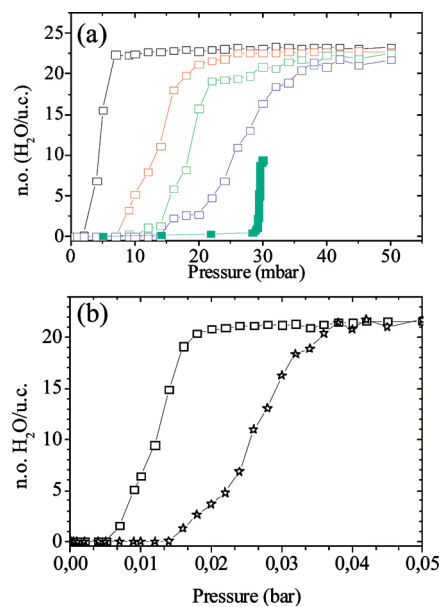


Figure 8. (a) Influence of the partial charges distribution (100% black; 70% red; 50% green; 30% blue) on the adsorption isotherm of MIL-47(V) at 300 K and comparison with the experimental data (cyan curve). (b) Comparison between the simulated adsorption isotherms for MIL-47(V) (stars) and for the LP form of MIL-53(Cr) (squares).

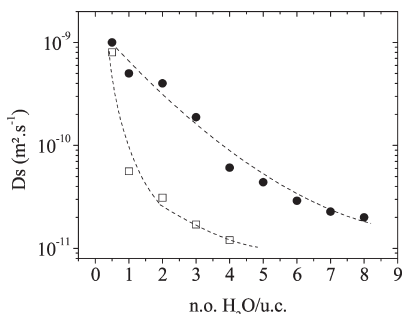


Figure 9. Self-diffusion coefficients for water calculated at 300 K in both the NP (empty squares) and the LP (solid circles) forms of MIL-53(Cr). The mean error bar for the simulated D_S is estimated to be 10%.

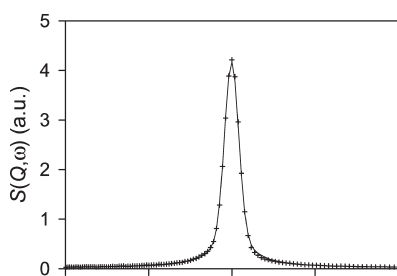


Figure 10. Comparison between experimental and fitted QENS spectra obtained at 300 K for H₂O in MIL-53(Cr). The solid line results from the convolution of a rotational diffusion model with the instrumental resolution (6 H₂O/u.c., Q = 1.35 Å⁻¹).

confinement degree is much higher in the NP structure. Further, these ranges of D_S values are lower than those obtained in the liquid state at 300 K, that is, 2.3×10^{-10} m²·s⁻¹, while in the LP form, they are slightly higher compared to the situation in other confined nanoporous solids including

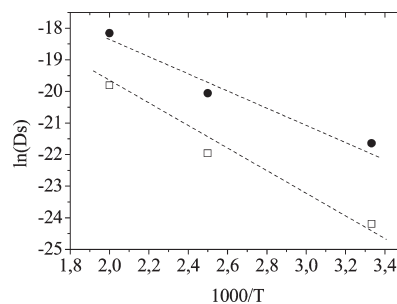


Figure 11. Arrhenius plots for extracting the activation energy for 2 H₂O/u.c at 300 K in both LP (solid circles) and NP (open squares) forms of MIL-53(Cr).

clays (1.4×10^{-10} m²·s⁻¹)^{91,92} and zeolites NaY (5.0×10^{-10} m²·s⁻¹ at 400 K).⁹³

A further step consisted of comparing these simulated data with those obtained by QENS measurements. The QENS spectra (Figure 10) can be analyzed only in terms of hydrogen motions, because of the large incoherent cross-section of this atom. In principle, such spectra contain information on both rotational and translational motions of water. However, by fitting the measured intensities by scattering functions corresponding to these two motions, it becomes clear that the translation was too slow to produce any quasi-elastic broadening. This implies that the self-diffusion coefficient of water is lower than 5×10^{-10} m²·s⁻¹, whatever the loading that is consistent with the range of values predicted by our simulations. Experiments with a higher energy resolution, such as those proposed by Paoli et al.,⁹⁴ would be necessary to characterize the translational diffusion of water in MIL-53(Cr). However, it was possible to derive a rotational diffusion coefficient, D_R, by fitting simultaneously all spectra. The so-obtained values range between 4 and 6×10^{10} s⁻¹, D_R being larger at smaller concentration. From simulations, the averaged correlation time for water molecules in the LP form is about 50 ps at low loading (1H₂O/u.c) while it reaches 2 ns at high loading (7H₂O/u.c) (Supporting Information Figures S2 and S3), which is within the same order of magnitude than those determined by PFG NMR in the case of alkanes in Cu-BTC.⁷⁴ Further, the D_R value calculated for 1 H₂O/u.c in the LP form is 1.4×10^{10} s⁻¹ within the same range of magnitude than those obtained by QENS but much lower than in the bulk water (1.5 ps and 60×10^{10} s⁻¹).⁹² In the case of the NP form, it is rather difficult to estimate such time as the high confinement strongly limits the degree of freedom of the water molecules.

The activation energies for the diffusion in both MIL-53(Cr) structures have been calculated for a loading of 2 H₂O/u.c by determining the diffusion coefficients at three temperatures (300, 400, and 500 K) (Figure 11). As already emphasized for other gases in this solid,^{67,71,95–97} the diffusion process is a temperature activated process and follows an Arrhenius law. Figure 11 reports activation energies of 39.5 and 29.8 kJ·mol⁻¹ for the NP and LP forms, respectively, that are within the same range of values than those previously observed in zeolites such as NaX (48 kJ·mol⁻¹) and NaY (35 kJ·mol⁻¹).⁹³ This trend is consistent with a faster diffusivity simulated in the LP form.

A further step consisted of analyzing the MD trajectories in order to provide a full picture of the diffusion mechanism in this material. Regarding the LP form, the diffusion process is found to be of 1D type as previously observed for other gases^{67,71,95–97} in the same form of this solid. An illustration is provided in Figure 12a

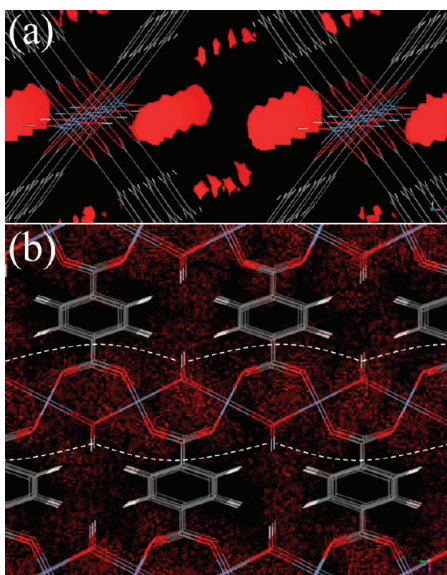


Figure 12. Typical illustration of the 1D microscopic diffusion mechanism of H₂O in the LP form of MIL-53(Cr) through the xz plane at (a) low loading (2 H₂O/uc) deduced from the 2D probability density plots extracted from the MD runs. Panel b illustrates the 1D type diffusion mechanism at high loadings through the xy plane, confirming the jump sequence between the $\mu_2\text{-OH}$ groups at low loadings through the xy plane, between the white dash lines.

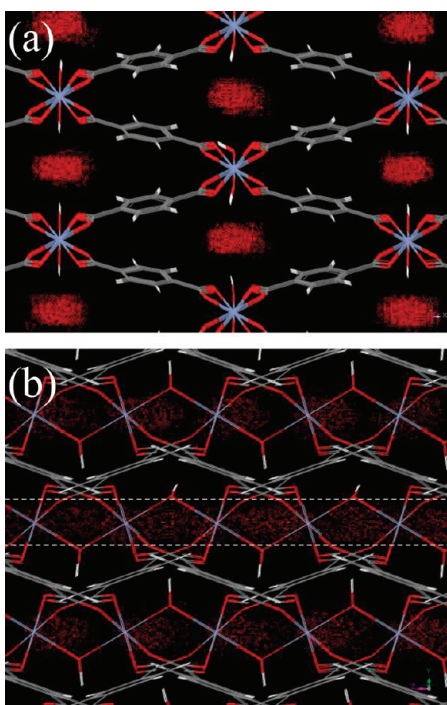


Figure 13. Typical illustration of the microscopic diffusion mechanism of H₂O in the NP form of MIL-53(Cr) through the xy plane at (a) low loading (2 H₂O/uc) and (b) through the xz plane at high loading (4 H₂O/uc) from the 2D probability density plots calculated by MD simulations.

where the trajectory of H₂O at low concentration in this LP form can be roughly drawn by following the higher density region provided by the 2D density plots. It is clearly observed that the

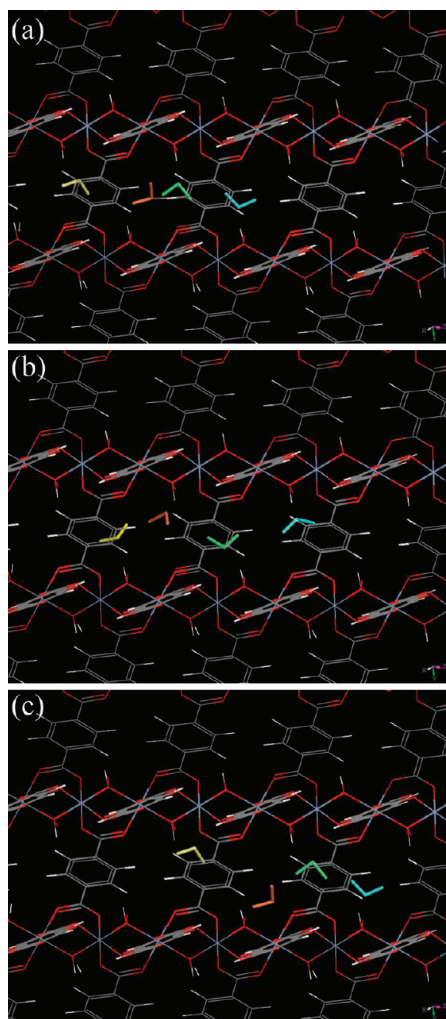


Figure 14. Illustration of the single-file diffusion mechanism in the NP form of MIL-53(Cr) through the xz plane (corresponding to the pore section); the sequence of the blue, yellow, and green water molecules is not modified as illustrated in the three snapshots extracted from the MD trajectory at different times corresponding to 0.5, 1, and 2 ns.

motions of the water are predominantly orientated along the direction of the tunnel, this behavior remaining true whatever the H₂O loading. Further, one can imagine (Figure 12a,b) a jump sequence between two consecutive $\mu_2\text{-OH}$ groups that act as steric barriers, the displacements along the two other axes being negligible with the absence of any density probability.

In contrast, the diffusion mechanism for water in the NP form is strongly confined in the middle of the pores; the displacements of the water molecules occur through a more restricted diffusion corridor involving simultaneous interactions with the two opposing sides of the same pore. This behavior is illustrated from the 2D density plots calculated in the NP form at low loading (1H₂O/uc) (see Figure 13a); the same situation is also observed at intermediate and higher loadings. Further, the 2D density plots represented through the xz plane (Figure 13b) suggests that the diffusion is more continuous along the direction of the tunnel rather than a jump sequence observed in the LP form. One can determine a diffusion corridor section of 5 Å, that is very similar to the ones we previously reported for other adsorbates molecules in such a material.⁹⁸ Because of the high confinement in

this NP structure, the water molecules tend to move via a single-file diffusion process, that is, the water molecules are not able to cross each other along the direction of the tunnel. This peculiar dynamical behavior is illustrated by three snapshots extracted from the MD trajectory for 2 H₂O/uc at different time intervals (Figures 14) which clearly show that the sequence of the water molecules along the tunnel remains the same along the simulation. Such an unusual diffusion type is consistent with what has already been evidenced in the case of CO₂ in the same NP form.⁷¹ Further analysis allowed us to estimate a mean residence time of the H₂O molecules around the μ_2 -OH groups for a loading of 2 H₂O/uc to be 50 ps in this NP form. As a comparison, this value is significantly higher than the one we previously determined for H₂ in the LP form (5 ps).⁹⁵

One should notice that the self-diffusivity for water is almost similar in both forms at very low loading (0.5 H₂O/uc). Such a behavior can be explained by the fact that the global diffusion mechanism of the water molecules is governed by two factors: the residence time spent by the water molecules close to the μ_2 -OH groups and the jump time required to pass from one μ_2 -OH group to another. Indeed, while the NP form leads to a shorter mean residence time than in the LP version, the jump time is longer. It results from these two opposite trends that the self-diffusivity is similar in both forms. The situation drastically differs for higher loadings; while the mean residence time remains similar in both forms, the jump times much strongly increase in the NP form due to the single file diffusion mechanism, thus leading to a deeper decrease of the self-diffusivity as observed in Figure 9.

CONCLUSION

After a careful validation of the force field for describing the interactions between the water and the flexible MIL-53(Cr) framework from a structural standpoint, the adsorption and diffusion mechanisms in both the large pore and the narrow pore forms of this structures were explored using appropriate molecular simulations combined with experimental data. It results that the breathing effect is accompanied by a modification of the hydrophobicity/hydrophilicity character of the MIL-53-(Cr) surface. While the LP form is mildly hydrophobic with the water molecules forming clusters in a similar way than in the bulk phase, the NP version is hydrophilic with strong interactions between the water molecules and the pore walls. A different dynamical behavior is also evidenced from our molecular dynamics simulations that show two different diffusion processes in the LP and the NP forms. While, the LP form imposes a 1D type diffusion mechanism for the water with jump sequence around the μ_2 -OH groups that act as steric barriers, the NP structure due to its high degree of confinement leads to slower diffusion process for water with a single-file 1D type mechanism. The structural switching opens a way to easily tune the hydrophobicity of MOFs to selectively adsorb organic pollutants or alcohols and could indeed partially explain its selective adsorption of alcohol in presence of water.³² Such a breathing effect can thus play a similar role than the functionalization of the structure with either hydrophobic or hydrophilic groups depending on the vapor/gas one aims at capturing. This strategy could lead to propose a low-cost adsorbent with high selectivity for the alcohols/water mixture.

ASSOCIATED CONTENT

S Supporting Information. Additional simulated data including Figures S1, S2, and S3. This material is available free of charge via the Internet at <http://pubs.acs.org>.

AUTHOR INFORMATION

Corresponding Author

*E-mail: guillaume.maurin@univ-montp2.fr.

ACKNOWLEDGMENT

This work was supported by French programs ANR CO₂ NoMAC (ANR-06-CO2-008). We thank the Institut Laue-Langevin, Grenoble, France, for the provision of neutron beam time and Dr. M. M. Koza for his help during the measurements on the IN6 spectrometer. We are very grateful to Dr. Qingyuan Yang from Beijing University of Chemical Technology for providing us the CADSS GCMC code.

REFERENCES

- (1) Long, J. R.; Yaghi, O. M. The Pervasive Chemistry of Metal-Organic Frameworks. *Chem. Soc. Rev.* **2009**, *38*, 1213–1214.
- (2) Férey, G. Hybrid Porous Solids. *Chem. Soc. Rev.* **2008**, *37*, 191–214.
- (3) Férey, G.; Serre, C. Large Breathing Effects in Three-Dimensional Porous Hybrid Matter: Facts, Analyses, Rules and Consequences. *Chem. Soc. Rev.* **2009**, *38*, 1380–1399.
- (4) Devic, T.; Horcajada, P.; Serre, C.; Salles, F.; Maurin, G.; Moulin, B.; Heurtault, D.; Clet, G.; Vimont, A.; Grenache, J. M.; Le Ouay, B.; Moreau, F.; Magnier, E.; Filinchuk, Y.; Marrot, J.; Lavalley, J. C.; Daturi, M.; Férey, G. Functionalization in Flexible Porous Solids: Effects of the Pore Opening and the Host–Guest Interactions. *J. Am. Chem. Soc.* **2010**, *132*, 1127–1136.
- (5) Mu, W.; Liu, D. H.; Yang, Q. Y.; Zhong, C. L. Computational Study of the Effect of Organic Linkers on Natural Gas Upgrading in Metal-Organic Frameworks. *Microporous. Mesoporous. Mater.* **2010**, *130*, 76–82.
- (6) Deng, H. X.; Doonan, C. J.; Furukawa, H.; Ferreira, R. B.; Towne, J.; Knobler, C. B.; Wang, B.; Yaghi, O. M. Multiple Functional Groups of Varying Ratios in Metal-Organic Frameworks. *Science* **2010**, *327*, 846–850.
- (7) Wang, Z.; Cohen, S. M. Modulating Metal–Organic Frameworks to Breathe: a Post-Synthetic Covalent Modification Approach. *J. Am. Chem. Soc.* **2009**, *131*, 16675–16677.
- (8) Choi, H. J.; Dinca, M.; Long, J. R. Broadly Hysteretic H₂ Adsorption in the Microporous Metal–Organic Framework Co(1,4-benzenedipyrrolo[1,4-c]quinoxaline-2,7-dione). *J. Am. Chem. Soc.* **2008**, *130*, 7848–7850.
- (9) Chae, H. K.; Siberio-Perez, D. Y.; Kim, J.; Go, Y.; Eddaoudi, M.; Matzgu, A. J.; O’Keeffe, M.; Yaghi, O. M. A Route to High Surface Area, Porosity and Inclusion of Large Molecules in Crystals. *Nature* **2004**, *427*, 523–527.
- (10) Salles, F.; Maurin, G.; Serre, C.; Llewellyn, P. L.; Knöfel, C.; Choi, H. J.; Long, J. R.; Filinchuk, Y.; Férey, G. Multi-Step Breathing in the Metal–Organic Framework Co(1,4-benzenedipyrrolo[1,4-c]quinoxaline-2,7-dione). *J. Am. Chem. Soc.* **2010**, *132* (39), 13782–13788.
- (11) Hamon, L.; Llewellyn, P. L.; Devic, T.; Ghoufi, A.; Clet, G.; Guillerm, V.; Pirngruber, G. D.; Maurin, G.; Serre, C.; Driver, G.; van Beek, W.; Jolimaitre, E.; Vimont, A.; Daturi, M.; Férey, G. Co-Adsorption and Separation of CO₂–CH₄ Mixtures in the Highly Flexible MIL-53(Cr) MOF. *J. Am. Chem. Soc.* **2009**, *131*, 17490–17499.
- (12) Hamon, L.; Leclerc, H.; Ghoufi, A.; Travert, A.; Lavalley, J. C.; Devic, T.; Serre, C.; Férey, G.; De Weireld, G.; Vimont, A.; Maurin, G. Molecular Insight into the Adsorption of H₂S in the Flexible MIL-53(Cr) and Rigid MIL-47(V) MOFs: Infrared Spectroscopy Combines to Molecular Simulations. *J. Phys. Chem. C* **2011**, *115*, 2047–2056.

- (13) Llewellyn, P. L.; Bourrelly, S.; Serre, C.; Vimont, A.; Daturi, M.; Hamon, L.; De Weireld, G.; Chang, J. S.; Hong, D. Y.; Hwang, Y. K.; Jhung, S. H.; Férey, G. High Uptakes of CO₂ and CH₄ in Mesoporous Metal–Organic Frameworks MIL-100 and MIL-101. *Langmuir* **2008**, *24*, 7245–7250.
- (14) Babarao, R.; Jiang, J. W. Exceptionally high CO₂ Storage in Covalent-Organic Frameworks: Atomic Simulation Study. *Energy Environ. Sci.* **2008**, *1*, 139–143.
- (15) Millward, A. R.; Yaghi, O. M. Metal–Organic Frameworks with Exceptionally High Capacity for Storage of Carbon Dioxide at Room Temperature. *J. Am. Chem. Soc.* **2005**, *127*, 17998–17999.
- (16) Demessence, A.; D’Alessandro, D. M.; Foo, M. L.; Long, J. R. Strong CO₂ binding in a Water-Stable Triazolate Bridged Metal–Organic Framework Functionalized with Ethylenediamine. *J. Am. Chem. Soc.* **2009**, *131*, 8784–8786.
- (17) Loiseau, T.; Serre, C.; Huguenard, C.; Fink, G.; Taulelle, F.; Henry, M.; Bataille, T.; Férey, G. A Rationale for the Breathing of the Porous Aluminum Terephthalate (MIL-53) upon hydration. *Chem.—Eur. J.* **2004**, *10*, 1373–1382.
- (18) Low, J. J.; Benin, A. I.; Jakubczak, P.; Abrahamian, J. F.; Faheem, S. A.; Willis, R. R. Virtual High Throughput Screening Confirmed Experimentally: Porous Coordination Polymer Hydration. *J. Am. Chem. Soc.* **2009**, *131*, 15834–15842.
- (19) Férey, G. Some Suggested Perspectives for Multifunctional Hybrid Porous Solids. *Dalton Trans.* **2009**, *23*, 4400–4415.
- (20) Czaja, A. U.; Trukhan, N.; Müller, U. Industrial Applications of Metal–Organic Frameworks. *Chem. Soc. Rev.* **2009**, *38*, 1284–1293.
- (21) Murray, L. J.; Dinca, M.; Long, J. R. Hydrogen Storage in Metal–Organic Frameworks. *Chem. Soc. Rev.* **2009**, *38*, 1294–1314.
- (22) Lee, J. Y.; Fartha, O. K.; Roberts, J.; Scheidt, K. A.; Nguyen, S. B. T.; Hupp, J. T. Metal–Organic Framework Materials as Catalysts. *Chem. Soc. Rev.* **2009**, *38*, 1450–1459.
- (23) Li, J. R.; Kuppler, R. J.; Zhou, H. C. Selective Gas Adsorption and Separation in Metal–Organic Frameworks. *Chem. Soc. Rev.* **2009**, *38*, 1477–1504.
- (24) Horcajada, P.; Chalati, T.; Serre, C.; Gillet, B.; Sebrie, C.; Baati, T.; Eubank, J. F.; Heurtaux, D.; Clayette, P.; Kreuz, C.; Chang, J. S.; Hwang, Y. K.; Marsaud, V.; Borie, P. N.; Cynober, L.; Gil, S.; Férey, G.; Couvreur, P.; Gref, R. Porous Metal–Organic Framework Nanoscale Carriers as a Potential Platform for Drug Delivery and Imaging. *Nat. Mater.* **2010**, *9*, 172–178.
- (25) Babarao, R.; Jiang, J. W. Unraveling the Energetics and Dynamics of Ibuprofen in Mesoporous Metal–Organic Frameworks. *J. Phys. Chem. C* **2009**, *113*, 18287–18291.
- (26) Horcajada, P.; Serre, C.; Maurin, G.; Ramsahye, N.; Balas, F.; Vallet-Regi, M.; Sebban, M.; Taulelle, F.; Férey, G. Flexible Porous Metal–Organic Frameworks for a Controlled Drug Delivery. *J. Am. Chem. Soc.* **2008**, *130*, 6774–6780.
- (27) Morris, R. E.; Wheatley, P. S. Gas Storage in Nanoporous Materials. *Angew. Chem., Int. Ed.* **2008**, *47*, 4966–4981.
- (28) Horcajada, P.; Serre, C.; Vallet-Regi, M.; Sebban, M.; Taulelle, F.; Férey, G. Metal–Organic Frameworks as Efficient Materials for Drug Delivery. *Angew. Chem., Int. Ed.* **2006**, *45*, 5974–5978.
- (29) Chen, Y. F.; Lee, J. Y.; Babarao, R.; Li, J.; Jiang, J. W. A Highly Metal–Organic Framework Zn(BDC)(TED)_{0.5} for adsorption and separation of CH₃OH/H₂O and CO₂/CH₄: an Integrated Experimental and Simulation Study. *J. Phys. Chem. C* **2010**, *114*, 6602–6609.
- (30) Bourrelly, S.; Llewellyn, P. L.; Serre, C.; Millange, F.; Loiseau, T.; Férey, G. Different Adsorption Behaviours of Methane and Carbon Dioxide in the Isotypic Nanoporous Metal Terephthalates MIL-53 and MIL-47. *J. Am. Chem. Soc.* **2005**, *127*, 13519–13521.
- (31) Zhang, J. P.; Chen, X.-M. Exceptional Framework Flexibility and Sorption Behaviour of a Multifunctional Porous Cuprous Triazolate Framework. *J. Am. Chem. Soc.* **2008**, *130*, 6010–6017.
- (32) Bourrelly, S.; Moulin, B.; Rivera, A.; Maurin, G.; Devautour-Vinot, S.; Serre, C.; Devic, T.; Horcajada, P.; Vimont, A.; Clet, G.; Daturi, M.; Lavallee, J. C.; Loera-Serna, S.; Denoyel, R.; Llewellyn, P. L.; Férey, G. An Explanation of The Adsorption of Polar Vapors in the Highly Flexible Metal–Organic Framework MIL-53(Cr). *J. Am. Chem. Soc.* **2010**, *132* (27), 9488–9498.
- (33) Llewellyn, P. L.; Bourrelly, S.; Serre, C.; Filinchuk, Y.; Férey, G. How Hydration Drastically Improves Adsorption Selectivity for CO₂ over CH₄ in the Flexible Chromium Terephthalate MIL-53. *Angew. Chem., Int. Ed.* **2006**, *45*, 7751–7754.
- (34) Han, S. S.; Choi, S. H.; van Duin, A. C. C. Molecular Dynamics Simulations of Stability of Metal–Organic Frameworks against H₂O using the ReaxFF Reactive Force Field. *Chem. Commun.* **2010**, *46*, 5713–5715.
- (35) Loiseau, T.; Mellot-Draznieks, C.; Muguerra, H.; Férey, G.; Haouas, M.; Taulelle, F. Hydrothermal Synthesis and Crystal Structure of a New Three-Dimensional Aluminum–Organic Framework MIL-69 with 2,6-Naphthalenedicarboxylate (ndc), Al(OH)(ndc).H₂O. *C.R. Chimie* **2005**, *8*, 765–772.
- (36) Saha, D.; Deng, S. Structural Stability of Metal–Organic Framework MOF-177. *J. Phys. Chem. Lett.* **2010**, *1*, 73–78.
- (37) Li, Y.; Yang, R. T. Gas Adsorption and Storage in Metal–Organic Framework MOF-177. *Langmuir* **2007**, *23*, 12937–12944.
- (38) Panella, B.; Hirscher, M. Hydrogen Physisorption in Metal–Organic Porous Crystals. *Adv. Mater.* **2005**, *17*, 538–541.
- (39) Greathouse, J. A.; Allenrdorf, M. D. The Interaction of Water with MOF-5 Simulated by Molecular Dynamics. *J. Am. Chem. Soc.* **2006**, *128*, 10678–10679.
- (40) Cheng, Y.; Kondo, A.; Nogucki, H.; Kajiro, H.; Uruta, K.; Ohba, T.; Kaneko, K.; Kanoh, H. Reversible Structural Change of Cu-MOF on Exposure to Water and its CO₂ adsorptivity. *Langmuir* **2009**, *25*, 4510–4513.
- (41) Comotti, A.; Bracco, S.; Sozzani, P.; Horike, S.; Matsuda, R.; Chen, J.; Takata, M.; Kubota, Y.; Kitagawa, S. Nanochannels of Two Distinct Cross-Sections in a Porous Al-Based Coordination Polymer. *J. Am. Chem. Soc.* **2008**, *130*, 13664–13672.
- (42) Chen, Y. F.; Babarao, R.; Sandler, S. I.; Jiang, J. W. Metal–Organic Framework MIL-101 for Adsorption and Effect of Terminal Water Molecules: from Quantum Mechanics to Molecular Simulations. *Langmuir* **2010**, *26*, 8743–8750.
- (43) Küsgens, P.; Rose, M.; Senkovska, I.; Fröde, H.; Henschel, A.; Siegle, S.; Kaskel, S. Characterization of Metal–Organic Framework by Water Adsorption. *Microporous. Mesoporous. Mater.* **2009**, *120*, 325–330.
- (44) Nalaparaju, A.; Zhao, X. S.; Jiang, J. W. Molecular Understanding for the Adsorption of Water and Alcohols in Hydrophilic and Hydrophobic Zeolitic Metal–Organic Frameworks. *J. Phys. Chem. C* **2010**, *114* (26), 11542–11550.
- (45) Devautour-Vinot, S.; Maurin, G.; Henn, F.; Serre, C.; Férey, G. Water and Ethanol Desorption in the Flexible Metal Organic Frameworks, MIL-53(Cr,Fe), Investigated by Complex Impedance Spectroscopy and Density Functional Theory Calculations. *Phys. Chem. Chem. Phys.* **2010**, *12*, 12478–12485.
- (46) Coombes, D. S.; Cora, F.; Mellot-Draznieks, C.; Bell, R. G. Sorption-Induced Breathing in the Flexible Metal–Organic Framework Cr-MIL53: Force Field Simulations and Electronic Structure Analysis. *J. Phys. Chem. C* **2009**, *113*, 544–552.
- (47) Dubbeldam, D.; Krishna, R.; Snurr, R. Q. Method for Analysing Structural Changes of Flexible Metal–Organic Frameworks Induced by Adsorbates. *J. Phys. Chem. C* **2009**, *113*, 19317–19327.
- (48) Ball, P. Chemical Physics: How to keep dry in water? *Nature* **2003**, *423*, 25–26.
- (49) Chandler, D. Hydrophobicity: Two Faces of water. *Nature* **2002**, *417*, 491.
- (50) Zhu, F. Q.; Schulten, K. Water and Proton Conduction through Carbon Nanotubes as Models for Biological Channels. *Biophys. J.* **2003**, *85*, 236–244.
- (51) Joseph, S.; Aluru, N. R. Pumping of Confined Water in Carbon Nanotubes by Rotation-Translation Coupling. *Phys. Rev. Lett.* **2008**, *101*, 064502.
- (52) Jobic, H. On the Jump Diffusion of Molecules in Zeolites Measured by Quasi-Elastic Neutron Scattering. *Microporous. Mesoporous. Mater.* **2002**, *55*, 159–169.

- (53) Zuo, G.; Shen, R.; Ma, S.; Guo, W. Transport Properties of Single-File Water Molecules inside a Carbon Nanotube Biomimicking Water Channel. *ACS Nano* **2010**, *4* (1), 205–210.
- (54) Ari, M. U.; Göktug Ahunbay, M.; Yurtsever, M.; Erdem-Senatalar, A. Molecular Dynamics Simulation of Water Diffusion in MFI-Type Zeolites. *J. Phys. Chem. B* **2009**, *113* (23), 8073–8079.
- (55) Cailliez, F.; Trzpit, M.; Soulard, M.; Demachy, I.; Boutin, A.; Patarin, J.; Fuchs, A. H. Thermodynamics of Water Intrusion in Nanoporous Hydrophobic Solids. *Phys. Chem. Chem. Phys.* **2008**, *10*, 4817–4826.
- (56) Marry, V.; Rotenberg, B.; Turq, P. Structure and Dynamics of Water at a Clay Surface from Molecular Dynamics Simulation. *Phys. Chem. Chem. Phys.* **2008**, *10*, 4802–4813.
- (57) Desbiens, N.; Demachy, I.; Fuchs, A. H.; Kirsch-Rodeschini, H.; Soulard, M.; Patarin, J. Water Condensation in Hydrophobic Nanopores. *Angew. Chem., Int. Ed.* **2005**, *44*, 5310–5313.
- (58) Paranthaman, S.; Coudert, F. X.; Fuchs, A. Water Adsorption in Hydrophobic MOF Channels. *Phys. Chem. Chem. Phys.* **2010**, *12*, 8123–8129.
- (59) Serre, C.; Millange, F.; Thouvenot, C.; Nogues, M.; Marsolier, G.; Louer, D.; Férey, G. Very Large Breathing Effect in the First Nanoporous Chromium (III) Based Solids: MIL-53 or Cr-III(OH)_x{O₂C-C₆H₄-CO₂}_y{HO₂C-C₆H₄-CO₂H}_x(H₂O)_y. *J. Am. Chem. Soc.* **2002**, *124*, 13519–13526.
- (60) Liu, Y.; Her, J. H.; Dailly, A.; Ramirez-Cuesta, A. J.; Neumann, D. A.; Brown, C. M. Reversible Structural Transition in MIL-53 with Large Temperature Hysteresis. *J. Am. Chem. Soc.* **2008**, *130*, 11813–11818.
- (61) Boutin, A.; Sringuel-Huet, M. A.; Nossov, A.; Gedeon, A.; Loiseau, T.; Volkinger, C.; Férey, G.; Coudert, F. X.; Fuchs, A. H. Breathing Transitions in MIL-53(Al) Metal-Organic Framework upon Adsorption. *Angew. Chem., Int. Ed.* **2009**, *48*, 8314–8317.
- (62) Neimark, A. V.; Coudert, F. X.; Boutin, A.; Fuchs, A. H. Stress-Based Model for the Breathing of Metal-Organic Frameworks. *J. Phys. Chem. Lett.* **2010**, *1*, 445–449.
- (63) (a) Serre, C.; Bourrelly, S.; Vimont, A.; Ramsahye, N. A.; Maurin, G.; Llewellyn, P. L.; Daturi, M.; Filinchuk, Y.; Leynaud, O.; Barnes, P.; Férey, G. An Explanation for the Very Large Breathing Effect of a Metal-Organic Framework during CO₂ Adsorption. *Adv. Mater.* **2007**, *19*, 2246–2251. (b) Llewellyn, P. L.; Maurin, G.; Devic, T.; Loera-Serna, S.; Rosenbach, N.; Serre, C.; Bourrelly, S.; Horcajada, P.; Filinchuk, Y.; Férey, G. Prediction of the Conditions for Breathing of Metal-Organic Framework Materials using a Combination of X-ray Powder Diffraction, Microcalorimetry and Molecular Simulations. *J. Am. Chem. Soc.* **2008**, *130*, 12808–12814.
- (64) Ghoufi, A.; Maurin, G. Hybrid Monte Carlo Simulations Combined with a Phase Mixture Model to Predict the Structural Transitions of a Porous Metal-Organic Framework Material upon Adsorption of Guest Molecules. *J. Phys. Chem. C* **2010**, *114*, 6496–6502.
- (65) Salles, F.; Ghoufi, A.; Maurin, G.; Bell, R. G.; Mellot-Draznieks, C.; Férey, G. Molecular Dynamics Simulations of Breathing MOFs: Structural Transformations of MIL-53(Cr) upon Thermal Activation and CO₂ Adsorption. *Angew. Chem., Int. Ed.* **2008**, *47*, 8487–8491.
- (66) Barthelet, K.; Marrot, J.; Riou, D.; Férey, G. A Breathing Hybrid Organic-Inorganic Solid with Very Large Pores and High Magnetic Characteristics. *Angew. Chem., Int. Ed.* **2002**, *41*, 281.
- (67) Rosenbach, N.; Jobic, H.; Ghoufi, A.; Salles, F.; Maurin, G.; Bourrelly, S.; Llewellyn, P. L.; Devic, T.; Serre, C.; Férey, G. Quasi-Elastic Neutron Scattering and Molecular Dynamics Study of Methane Diffusion in Metal-Organic Frameworks MIL-47(V) and MIL-53(Cr). *Angew. Chem., Int. Ed.* **2008**, *47*, 6611–6615.
- (68) Abascal, J. L. F.; Vega, C. A General Purpose Model for the Condensed Phases of Water: TIP4P/2005. *J. Chem. Phys.* **2005**, *123*, 234505.
- (69) Smith, W.; Forester, T. R. DL_POLY_2.0: A General-Purpose Parallel Molecular Dynamics Simulation Package. *J. Mol. Graph.* **1996**, *14*, 136–141.
- (70) Ewald, P. Die Berechnung optischer und elektrostatischer Gitterpotentiale. *Ann. Phys.* **1921**, *369*, 253–287.
- (71) Salles, F.; Jobic, H.; Ghoufi, A.; Llewellyn, P. L.; Serre, C.; Bourrelly, S.; Férey, G.; Maurin, G. Transport Diffusivity of CO₂ in the Highly Flexible Metal-Organic Framework MIL-53(Cr). *Angew. Chem., Int. Ed.* **2009**, *48*, 8335–8339.
- (72) Frenkel, D.; Smit, B. *Understanding Molecular Simulation*; Academic Press: San Diego, CA, 1996.
- (73) Saengsawang, O.; Schuring, A.; Remsungen, T.; Loiruangsins, A.; Hannongbua, S.; Magusin, P. C. M. M.; Fritsche, S. Rorational Motion of Pentant in the Flat γ Cages of Zeolites KFI. *J. Phys. Chem. C* **2008**, *112* (15), 5922–5929.
- (74) Wehring, M.; Gascon, J.; Dubbeldam, D.; Kapteijn, F.; Snurr, R. Q.; Stallmach, F. Self-Diffusion Studies in Cu-BTC by PFG NMR and MD Simulations. *J. Phys. Chem. C* **2010**, *114*, 10527–10534.
- (75) Yang, Q.; Zhong, C. Molecular Simulation of Carbon Dioxide/Methane/Hydrogen Mixture Adsorption in Metal-Organic Frameworks. *J. Phys. Chem. B* **2006**, *110*, 17776–17783.
- (76) Guillou, N.; Millange, F.; Walton, R. I. Rapid and Reversible Formation of a Crystalline Hydrate of a Metal-Organic Framework Containing a Tube of Hydrogen-bonded Water. *Chem. Commun.* **2011**, *47*, 713–715.
- (77) Poling, B. E.; Prausnitz, J. M.; O'Connell, J. P. *The Properties of Gases and Liquids*, 5th ed.; McGraw-Hill: New-York, 2001.
- (78) Cailliez, F.; Stirnemann, G.; Boutin, A.; Demachy, I.; Fuchs, A. H. Does Water Condense in Hydrophobic Cavities? A Molecular Simulation Study of Hydration in Heterogeneous Nanopores. *J. Phys. Chem. C* **2008**, *112*, 10435–10445.
- (79) Mir, M. H.; Wang, L.; Wong, M. W.; Vittal, J. J. Water Helicate (H₂O)₇ Hosted by a Diamondoid Metal-Organic Framework. *Chem. Commun.* **2009**, 4539–4541.
- (80) Duan, C.; Wei, M.; Guo, D.; He, C.; Meng, Q. Crystal Structures and Properties of Large Protonated Water Clusters Encapsulated by Metal-Organic Frameworks. *J. Am. Chem. Soc.* **2010**, *132*, 3321–3330.
- (81) Krishna, R.; van Baten, J. Highlighting a Variety of Unusual Characteristics of Adsorption and Diffusion in Microporous Materials Induced by Clustering of Guest Molecules. *Langmuir* **2010**, *26*, 8450–8463.
- (82) Trzpit, M.; Soulard, M.; Patarin, J.; Desbiens, N.; Cailliez, F.; Boutin, A.; Demachy, I.; Fuchs, A. H. The Effect of Local Defects on Water Adsorption in Silicalite-1 Zeolite: A Joint Experimental and Molecular Simulation Study. *Langmuir* **2007**, *23*, 10131–10139.
- (83) Demontis, P.; Gulin-Gonzalez, J.; Jobic, H.; Masia, M.; Sale, R.; Suffritti, G. B. Dynamical properties of confined water nanoclusters: simulation study of hydrated zeolite NaA: structural and vibrational properties. *ACS Nano* **2008**, *2*, 1603–1614.
- (84) Rouquerol, J.; Rouquerol, F.; Sing, K. S. W. *Adsorption by Powders and Porous Solids: Principles, Methodology and Applications*; Academic Press: New York, 1999.
- (85) Ludwig, R. Water: From Clusters to the Bulk. *Angew. Chem., Int. Ed.* **2001**, *40*, 1808–1827.
- (86) Jorgensen, W. L.; Jenson, C. Temperature Dependence of TIP3P, SPC, and TIP4P Water from NPT Monte Carlo Simulations: Seeking Temperatures of Maximum Density. *J. Comput. Chem.* **1998**, *19*, 1179–1186.
- (87) Flanigen, E. M.; Bennet, J. M.; Grose, R. W.; Cohen, J. P.; Patton, R. L.; Kirshner, R.; Smith, J. V. Silicalite, a New Hydrophobic Crystalline Silica Molecular-Sieve. *Nature* **1978**, *271*, 512–516.
- (88) Desbiens, N.; Boutin, A.; Demachy, I. Water Condensation in Hydrophobic Silicalite-1 Zeolite: A Molecular Simulation Study. *J. Phys. Chem. B* **2005**, *109*, 24071–24076.
- (89) Bordat, P.; Cazade, P. A.; Baraille, I.; Brown, R. Host and Adsorbate Dynamics in Silicalites with Flexible Frameworks: Empirical Force Field Simulation of Water in Silicalite. *J. Chem. Phys.* **2010**, *132*, 094501.
- (90) Castillo, J. M.; Vlugt, T. J. H.; Calero, S. Molecular Simulation Study on the Separation of Xylene Isomers in MIL-47 Metal-Organic Frameworks. *J. Phys. Chem. C* **2009**, *113*, 20869–20874.
- (91) Marry, V.; Turq, P.; Cartailler, T.; Levesque, D. Microscopic Simulation of Structure and Dynamics of Water and Counterions in a Monohydrated Montmorillonite. *J. Chem. Phys.* **2002**, *117*, 3454–3463.

- (92) Michot, L. J.; Delville, A.; Humbert, B.; Plazanet, M.; Levitz, P. Diffusion of Water in a Synthetic Clay with Tetrahedral Charges by Combined Neutron Time-of-Flight Measurements and Molecular Dynamics simulations. *J. Phys. Chem. C* **2007**, *111*, 9818–9831.
- (93) Demontis, P.; Jobic, H.; Gonzalez, M. A.; Suffritti, G. B. Diffusion of Water in Zeolites NaX and NaY Studied by Quasi-Elastic Neutron Scattering and Computer Simulation. *J. Phys. Chem. C* **2009**, *113*, 12373–12379.
- (94) Paoli, H.; Méthivier, A.; Jobic, H.; Krause, C.; Pfeifer, H.; Stallmach, F.; Kärger, J. Comparative QENS and PFG NMR Diffusion Studies of Water in Zeolite NaCaA. *Microporous. Mesoporous. Mater.* **2002**, *55*, 147.
- (95) Salles, F.; Jobic, H.; Maurin, G.; Koza, M. M.; Llewellyn, P. L.; Devic, T.; Serre, C.; Férey, G. Experimental Evidence Supported by Simulations of a Very High H₂ Diffusion in Metal-Organic Framework Materials. *Phys. Rev. Lett.* **2008**, *100*, 245901.
- (96) Salles, F.; Kolokolov, D. I.; Jobic, H.; Maurin, G.; Llewellyn, P. L.; Devic, T.; Serre, C.; Férey, G. Adsorption and Diffusion of H₂ in the MOF type systems MIL-47(V) and MIL-53(Cr): a Combination of Microcalorimetry and QENS Experiments with Molecular Simulations. *J. Phys. Chem. C* **2009**, *113*, 7802–7812.
- (97) Salles, F.; Jobic, H.; Devic, T.; Llewellyn, P. L.; Serre, C.; Férey, G.; Maurin, G. Self and Transport Diffusivity of CO₂ in the Metal–Organic Framework MIL-47(V) explored by Quasi-Elastic Neutron Scattering Experiments and Molecular Dynamics Simulations. *ACS Nano* **2010**, *4*, 143–152.
- (98) Jobic, H.; Rosenbach, N.; Ghoufi, A.; Kolokolov, D. I.; Yot, P. G.; Devic, T.; Serre, C.; Férey, G.; Maurin, G. Unusual Chain-Length Dependence of the Diffusion of n-Alkanes in the Metal-Organic Framework MIL-47(V): the Blowgun Effect. *Chem.—Eur. J.* **2010**, *16*, 10337–10341.